Supplementary Information - Active Particle Doping Suppresses Brittle Failure in Ultrastable Glasses

Rashmi Priya[1],[1] Jürgen Horbach[2],[1] and Smarajit Karmakar[11,*]

[11] *Tata Institute of Fundamental Research, 36/P, Gopanpally Village, Serilingampally Mandal, Ranga Reddy District, Hyderabad, India 50046*

[2] *Institut für Theoretische Physik II - Soft Matter, Heinrich-Heine-Universität, Düsseldorf, Germany*

I. SHEARED ULTRASTABLE GLASS IN 3D

In Fig. 1, we show the mechanical response of an ultrastable glass under shear for two system sizes, $10,000\,(10k)$ and $100,000\,(100k)$, in 3D. Figure (a) shows the stress-strain curves at two different strain rates, $\dot{\gamma} = 1 \times 10^{-4}, 5 \times 10^{-5}$. In (b) and (c), we plot the system's potential per particle and susceptibility. We show that the system exhibits shear-thinning behavior, characterized by the Herschel–Bulkley model with a flow index less than 1.

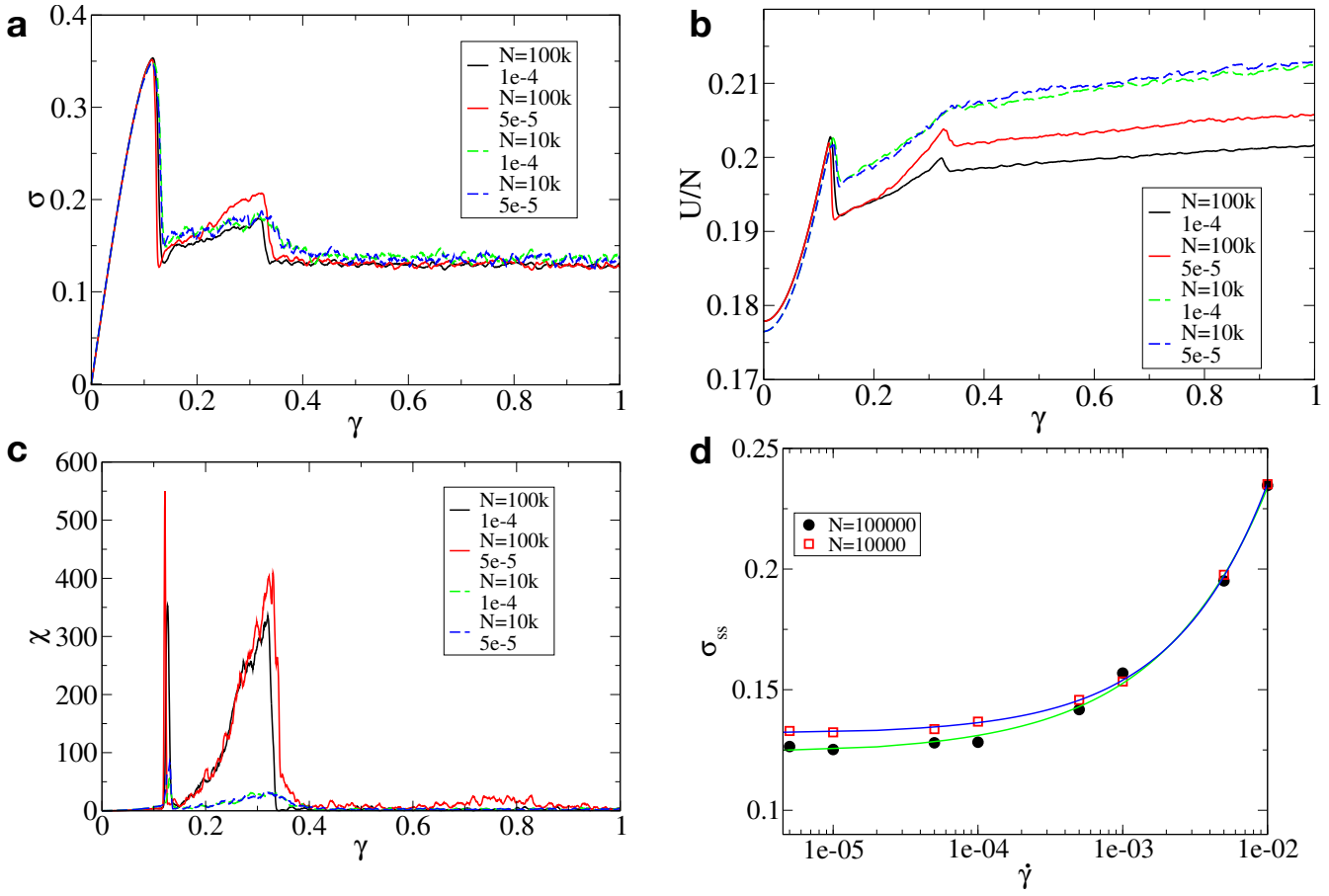

FIG. 1. **Ultrastable Glassy System in 3D:** Figure (a), (b), and (c) present the stress-strain curve, potential energy per particle, and susceptibility, respectively, for two different system sizes. The dotted line corresponds to $N = 10k$, and the solid line to $N = 100k$. In Figure (d), we plot the Herschel-Bulkley curve for both cases, demonstrating shear-thinning behavior consistent with findings from previous studies.

* smarajit@tifrh.res.in

II. MECHANICAL RESPONSE OF ULTRASTABLE GLASS IN THE PRESENCE OF SELF-PROPELLED PARTICLES

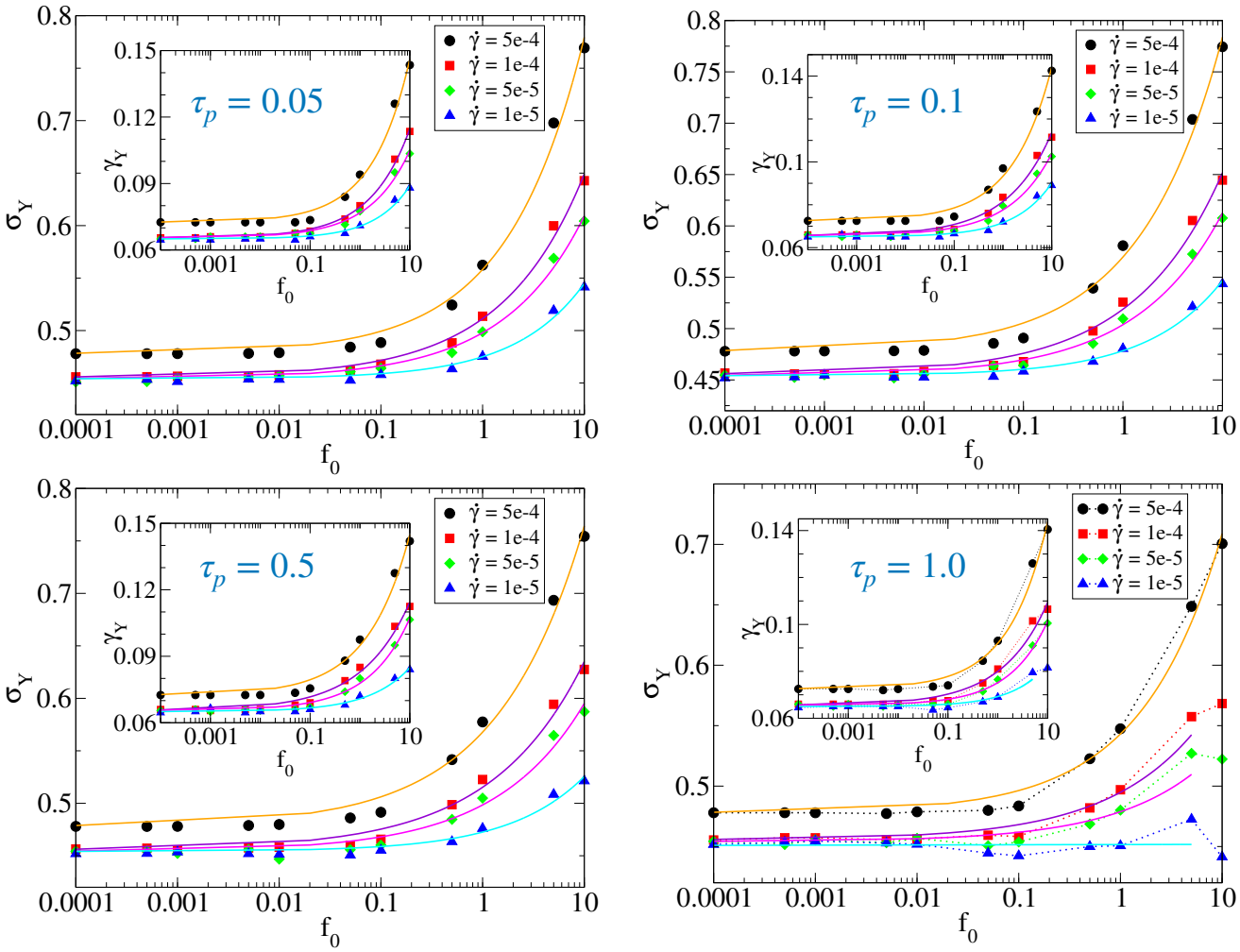

FIG. 2. **Strain Rate Dependence of Yielding at Different τ_p:** For lower τ_p values $(0.05, 0.1, 0.5)$, the system exhibits shear-thinning behavior with activity across all strain rates studied, as shown in (a), (b), and (c) (for the 2D case). As τ_p increases to 1.0, the yield stress at lower strain rates initially rises with increasing f_0 in the intermediate regime; however, further increases in f_0 cause the yield stress to decrease.

We show the shear thinning behavior for different persistence times $(0.05, 0.1, 0.5)$ and strain rates $(5 \times 10^{-4}, 1 \times 10^{-4}, 5 \times 10^{-5}, 1 \times 10^{-5})$ in Fig. 2. As persistence time increases to $\tau_P = 1.0$, we observe an increase in yield stress followed by a decrease at $\dot{\gamma} = 5 \times 10^{-5}, 1 \times 10^{-5}$, indicating a non-monotonic behavior of yield stress with increasing f_0. Nevertheless, shear thinning behavior is still observed at faster strain rates. As τ_p increases further, the strain rate range over which the enhanced mechanical response is observed decreases.

The non-monotonic effect with increasing f_0 becomes more pronounced at lower strain rates, where slower deformation allows shear band propagation, while faster strain rates inhibit it. Increasing τ_p further at higher f_0 facilitates rearrangements and stress release, leading to a reduction in yield stress.

After studying the yielding behavior, it becomes essential to investigate the flow characteristics of the system, particularly in the steady-state regime, where transient effects have relaxed and the system's stress fluctuates around a well-defined mean. To assess whether the system has reached this steady state, we analyze the potential energy, which serves as a sensitive measure of structural relaxation. When the potential energy plateaus, it indicates that the system has stabilized. We therefore plot the potential energy for larger system sizes ($N = 10^4$ in 2D and $N = 10^5$ in 3D) and observe that within the accessible deformation window, the potential energy continues to increase, suggesting that these systems have not yet reached steady state and may require much larger strains to do so. To overcome this

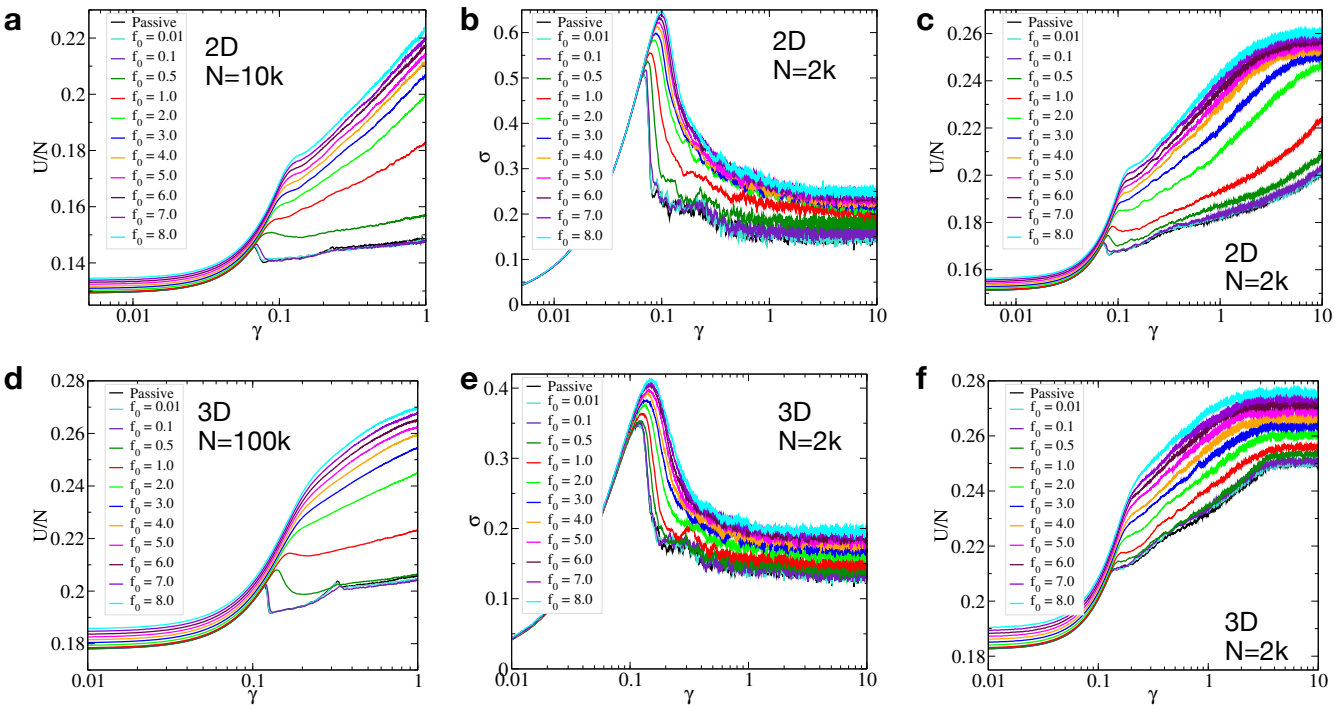

FIG. 3. **Steady State Analysis in Two and Three Dimensions:** This figure demonstrates that system size plays a crucial role in reaching a steady state. Panels (a) and (d) show that the potential energy for 2D and 3D systems with $N = 10^4$ and $N = 10^5$ continues to increase, indicating that these systems remain far from steady state. Therefore, we examine a smaller system size ($N = 2000$) in both 2D and 3D, and plot the stress and potential energy responses with increasing strain in panels (b) and (c) for 2D, and panels (e) and (f) for 3D. In 2D, we observe that while the stress plateaus, the potential energy continues to increase for lower active forces. However, as f_0 increases, the system reaches steady state more rapidly in both dimensions. This acceleration occurs due to the formation of multiple shear bands that span the system more easily when the network structure is homogeneously distributed throughout the system. In contrast, the 3D system clearly achieves a well-defined steady state across all measured quantities and is therefore better suited for studying steady-state behavior in active ultrastable systems.

limitation, we consider a smaller system size ($N = 2000$) in both 2D and 3D and examine the stress and potential energy response up to a large strain of $\gamma = 10.0$. We find that in 3D, both the stress and potential energy stabilize, indicating a clear steady state. In 2D, while the stress reaches a plateau, the potential energy continues to rise, particularly at lower active forces (f_0), including the passive case—likely due to the system-spanning shear bands or less branched network structures. Based on these observations, the 3D system with $N = 2000$ is well-suited for studying the flow curve, as it reliably reaches a steady state within accessible deformation.

III. SHEAR BAND EVOLUTION WITH INCREASING ACTIVITY

We first show a binary mapping of the system to a replica, which is used for all shear band analyses. In 2D, the system is divided into small cells, and in 3D, it is divided into small cubes. The non-affine displacements of particles within each cell or cube are quantified using D^2_{min}. A cell or cube is classified as part of the shear band region (marked in red) if its local D^2_{min} exceeds a predefined cutoff in reduced Lennard-Jones (LJ) units, with the cell size scaled to unit box length. Otherwise, it is considered outside the shear band region as shown in blue. Using this method, we generate a binary image that replicates the shear band regions, as illustrated in Fig. 4 (b) and (d).

We also show shear band evolution at two additional strain rates $\dot{\gamma} = 1 \times 10^{-4}, 1 \times 10^{-5}$ at $\tau_p = 0.1$, where we observe that as f_0 increases, the network of shear bands becomes denser as shown in Fig. 5 and Fig. 6. At faster strain rates, $\dot{\gamma} = 1 \times 10^{-4}$, a smaller self-propulsion force, $f_0 = 1.0$ is sufficient to produce multiple shear bands, whereas at slower deformation rate, $\dot{\gamma} = 1 \times 10^{-5}$, a higher value of active force, $f_0 \geq 8.0$ is required to form similar networks.

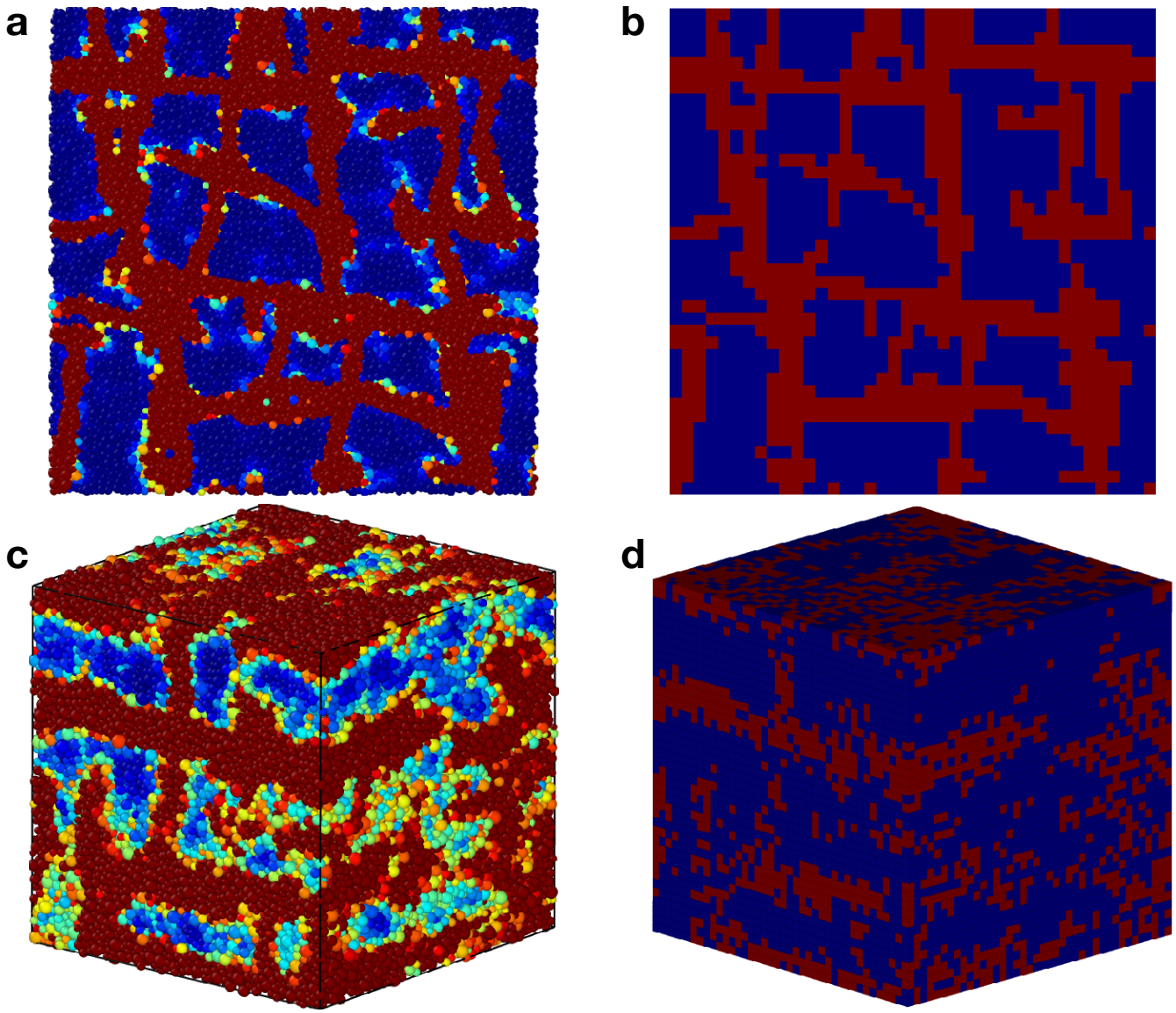

FIG. 4. **Binary Mapping of System in 2D and 3D**: The images shown in (b) and (d) are binary representations of the actual systems shown in (a) and (c) in 3D and 2D, respectively. The region in red correspond to shear bands, while regions lie outside the shear bands.

IV. SCALING OF YIELD STRESS WITH STRAIN RATE AND ACTIVE FORCE

In Fig. 7, we show the collapse of yield stress data presented in Fig. 2 with increasing f_0, at different strain rates for different persistence times in 2D. We observe a strong collapse for $\tau_p = 0.05, 0.1, 0.5$ when the x-axis is rescaled to $\dot{\gamma} f_0^{1.75}$. The y-axis is modified yield stress σ_Y^* given by:

$$\sigma_Y^* = \sigma_Y(\dot{\gamma}, f_0) - \sigma_{AQS}^P - \alpha_0 \dot{\gamma}^{\beta_0} \tag{1}$$

where σ_{AQS}^P, α_0 and β_0 are deduced from Fig 1.

$$\sigma_Y^* = \alpha(\dot{\gamma} f_0^m)^\beta \tag{2}$$

The data follows the eq. 2, where $\alpha = 1.0$ and $\beta < 1$, which can be expressed in its final form as:

$$\sigma_Y(\dot{\gamma}, f_0) = \sigma_{AQS}^P + \alpha_0 \dot{\gamma}^{\beta_0} + \alpha(\dot{\gamma} f_0^m)^\beta, \tag{3}$$

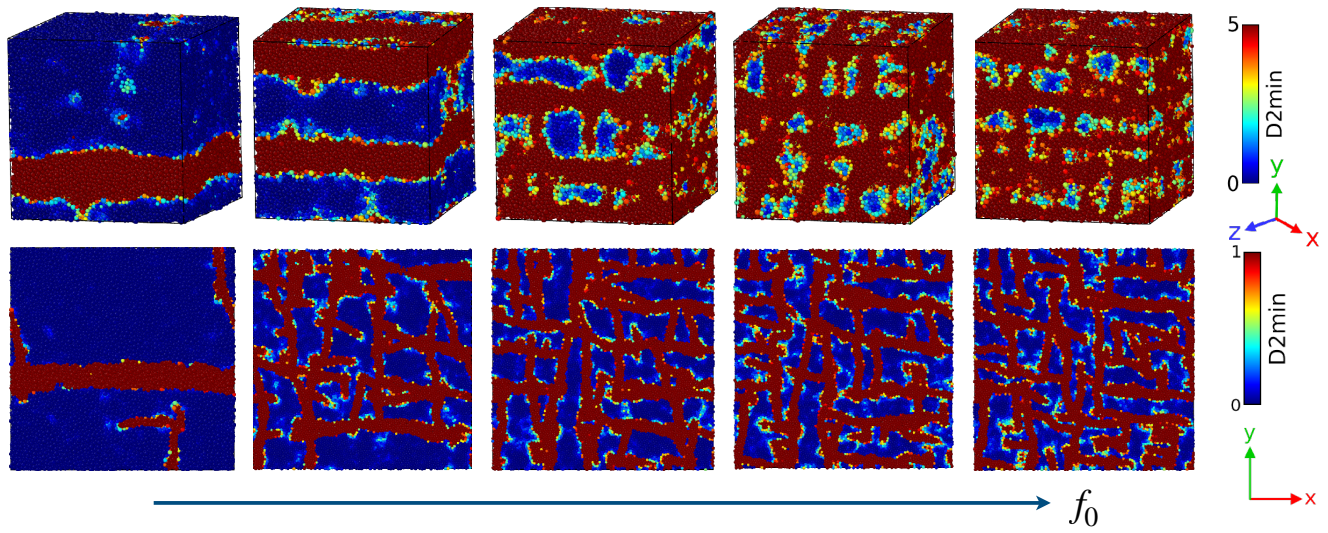

FIG. 5. **Shear band at $\dot{\gamma} = 1 \times 10^{-4}$ and $\tau_p = 0.1$:** Evolution of shear band with increasing f_0 values $0.0, 1.0, 2.0, 3.0, 4.0$ at $\tau_p = 0.1$, strain rate $\dot{\gamma} = 1 \times 10^{-4}$ and strain $\gamma = 0.20$ in 2D and 3D.

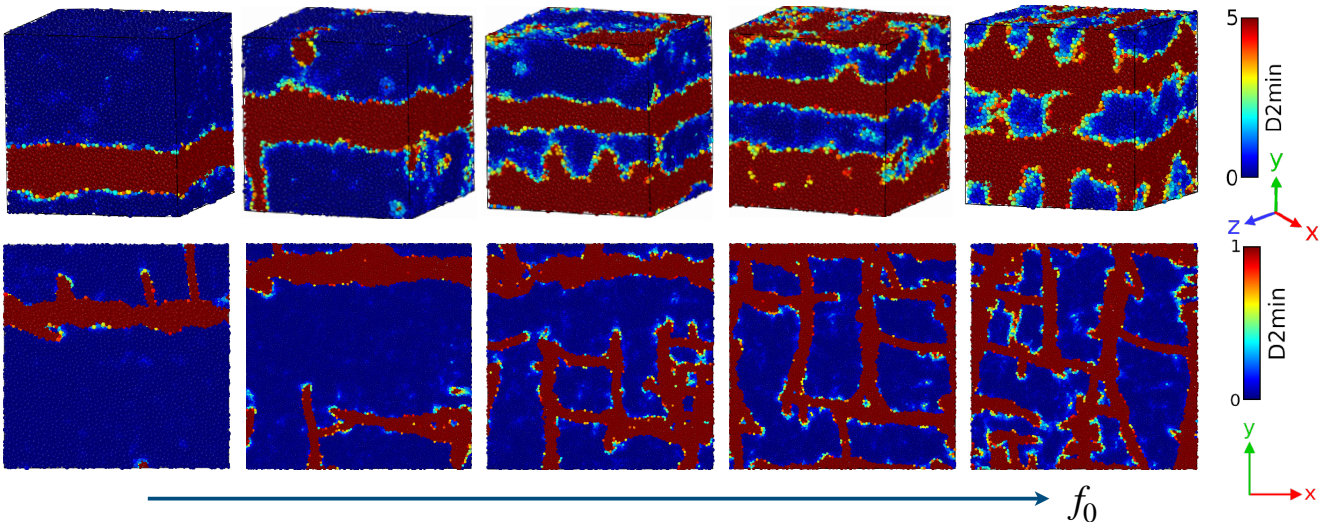

FIG. 6. **Shear band at $\dot{\gamma} = 1 \times 10^{-5}$ and $\tau_p = 0.1$:** Evolution of shear band with increasing f_0 values $0.0, 1.0, 2.0, 3.0, 4.0$ at $\tau_p = 0.1$, strain rate $\dot{\gamma} = 1 \times 10^{-5}$ and $\gamma = 0.20$ in 2D and $\gamma = 0.40$ in 3D.

However, as τ_p increases to 1.0, the collapse begins to deviate slightly, since at lower strain rates, increasing activity decreases yield stress, as discussed above. The observed collapse reinforces that the interplay between $\dot{\gamma}$ and f_0 governs the yield stress behavior across different persistence times.

V. YIELDING BEHAVIOR ACROSS ENSEMBLES IN ISOMORPHIC SYSTEMS

We present the stress-strain curve for different ensembles corresponding to two distinct pairs of isomorphs.

- $(\dot{\gamma} = 5 \times 10^{-4},\ f_0 = 1.0)$,$(\ \dot{\gamma} = 5 \times 10^{-5},\ f_0 = 6.0)$
- $(\dot{\gamma} = 5 \times 10^{-4},\ f_0 = 2.0)$,$(\ \dot{\gamma} = 1 \times 10^{-4},\ f_0 = 8.0)$.

The results show that the yielding behavior of an ensemble for a pair of isomorphs is exactly the same. However, beyond the yield point, the responses start to deviate due to the formation of multiple shear band networks. This

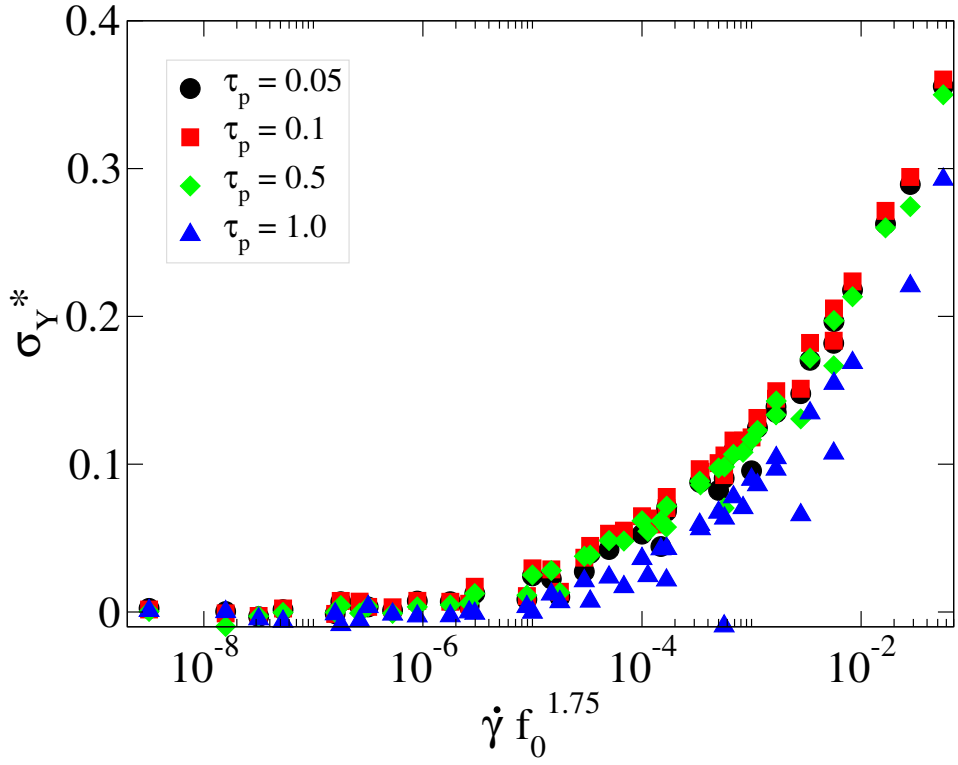

FIG. 7. **Yield Stress Collapse Across Different Persistence Times:** We demonstrate that the yield stress data for all values of $\tau_p = 0.05, 0.1, 0.5, 1.0$ exhibit a collapse onto a single curve for each τ_p when the x-axis is rescaled as $\dot{\gamma} f_0^{1.75}$ (in 2D). For $\tau_p = 1.0$, the data start deviating from collapse because a low strain rate and high f_0 lead to a non-monotonic increase followed by a decrease in yield stress, as observed in Fig. 2.

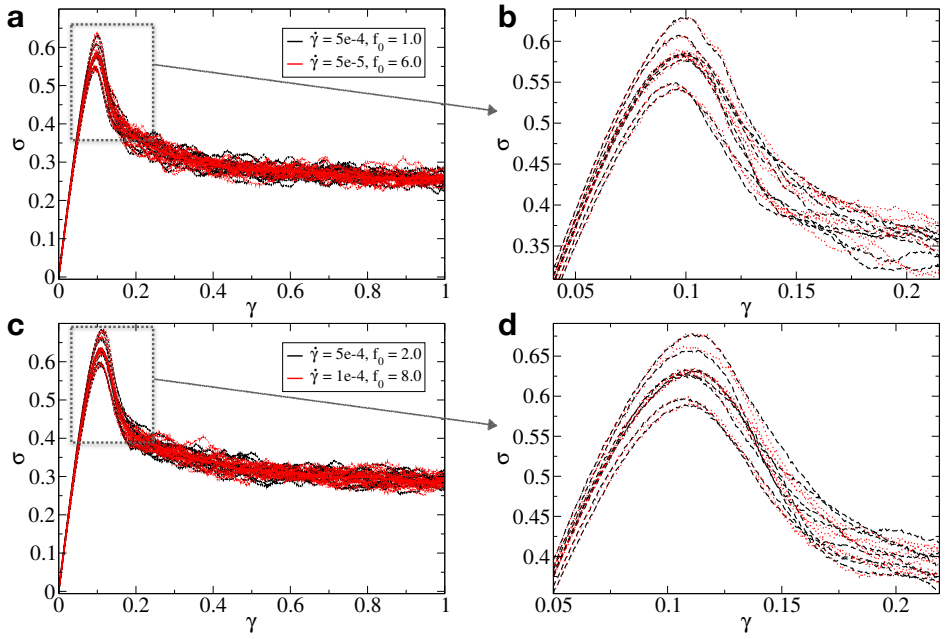

FIG. 8. **Stress-Strain Response for Two Isomorphs:** The stress-strain curve for two isomorphic curves is plotted for all ensembles (in 2D for $N = 10000$), demonstrating similar yielding behavior before and after the yield point. As the system approaches a steady state, the stress values fluctuate around the mean.

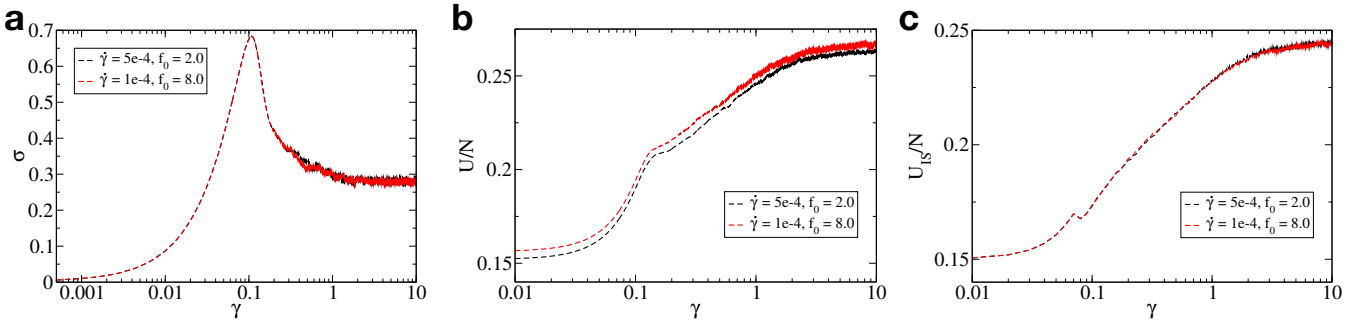

FIG. 9. **Isomorphs in steady-state:** In this figure, we show the steady-state behavior of a system with size $N = 2000$ in 2D. Under larger deformation, the system's stress, potential energy, and inherent state energy reach a steady state. We demonstrate that, in the steady state, the stress and inherent state energy remain the same for two different combinations of $\dot{\gamma}$ and f_0, whereas the potential energy differs.

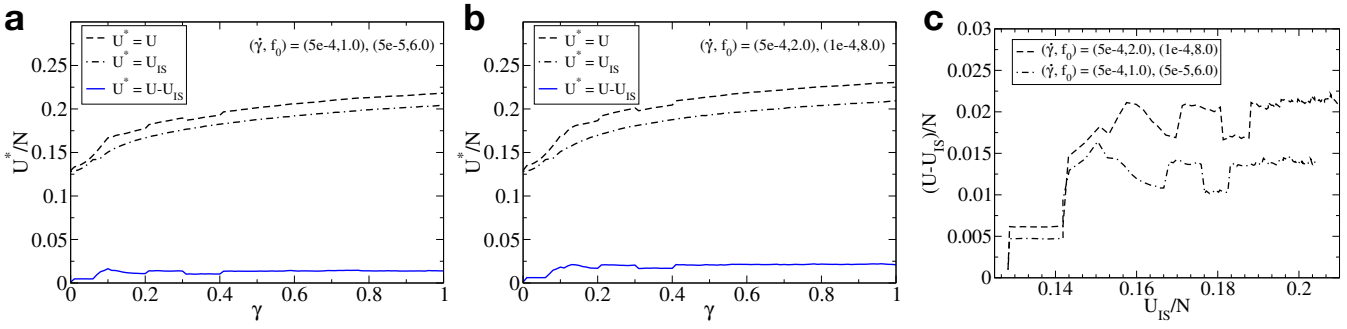

FIG. 10. In this figure, we quantify the difference between the potential energy and the inherent-state energy for two isomorphic cases (in 2D for $N = 10000$): $(\dot{\gamma}, f_0) = (5\times10^{-4}, 1.0), (5\times10^{-5}, 6.0)$ and $(\dot{\gamma}, f_0) = (5\times10^{-4}, 2.0), (1\times10^{-4}, 8.0)$. Panels (a) and (b) show the potential energy, the inherent-state energy, and their difference $(U^* = (U - U_{IS}))$ while switching at intervals of 0.1, 0.2, 0.3, and 0.4 from one pair to the other for both cases. The difference follows a pattern similar to that of the potential energy, and when this difference is plotted against the inherent-state energy, $(U - U_{IS})/N$ jumps to a new plateau and then remains constant within that state until the next switch.

deviation occurs because both the polydispersity of the system and the random selection of 20% active particles lead to different spatial distributions of active particles between isomorphs.

We also show that the behavior remains the same even when the system reaches steady state. For this, we consider a smaller system size $N = 2000$ in 2D, where the system reaches steady state under larger deformation $\gamma = 10.0$. We examine the evolution of stress, potential energy and inherent state energy responses of the isomorphs: $\dot{\gamma} = 5 \times 10^{-4}$, $f_0 = 2.0$),($\dot{\gamma} = 1 \times 10^{-4}$, $f_0 = 8.0$ with strain, as shown in Fig. 9.

We also show the difference in potential energy and inherent state energy in Fig. 10 for $N = 10000$ in 2D, and observe that when switching from one combination of $(\dot{\gamma}, f_0) = (5 \times 10^{-4}, 1.0), (5 \times 10^{-5}, 6.0)$ to another $(\dot{\gamma}, f_0) = (5 \times 10^{-4}, 2.0), (1 \times 10^{-4}, 8.0)$, the difference exhibits a jump at the switching point and remains constant otherwise.

VI. NON-MONOTONIC MECHANICAL RESPONSE

We observe a non-monotonic behavior in the yield stress of the ultrastable glasses under deformation in the presence of self-propelled particles. In Fig. 11, we show stress-strain curves for different strain rates, $\dot{\gamma} = 5\times10^{-4}, 1\times10^{-4}, 1\times10^{-5}$, highlighting that the non-monotonic behavior is consistently observed at $\tau_p = 0.1$ across all cases. However, with increasing strain rate, there is a shift to a higher value in both the persistence time at which yield stress overshoots the passive case and the persistence time at which $\sigma_Y \to 0$.

To further illustrate this, we plot yield stress as a function of τ_p in Fig. 12, shown in both 2D (top panel) and 3D (bottom panel). In (b) and (e), only three selected data points are shown, along with a dotted line extending from

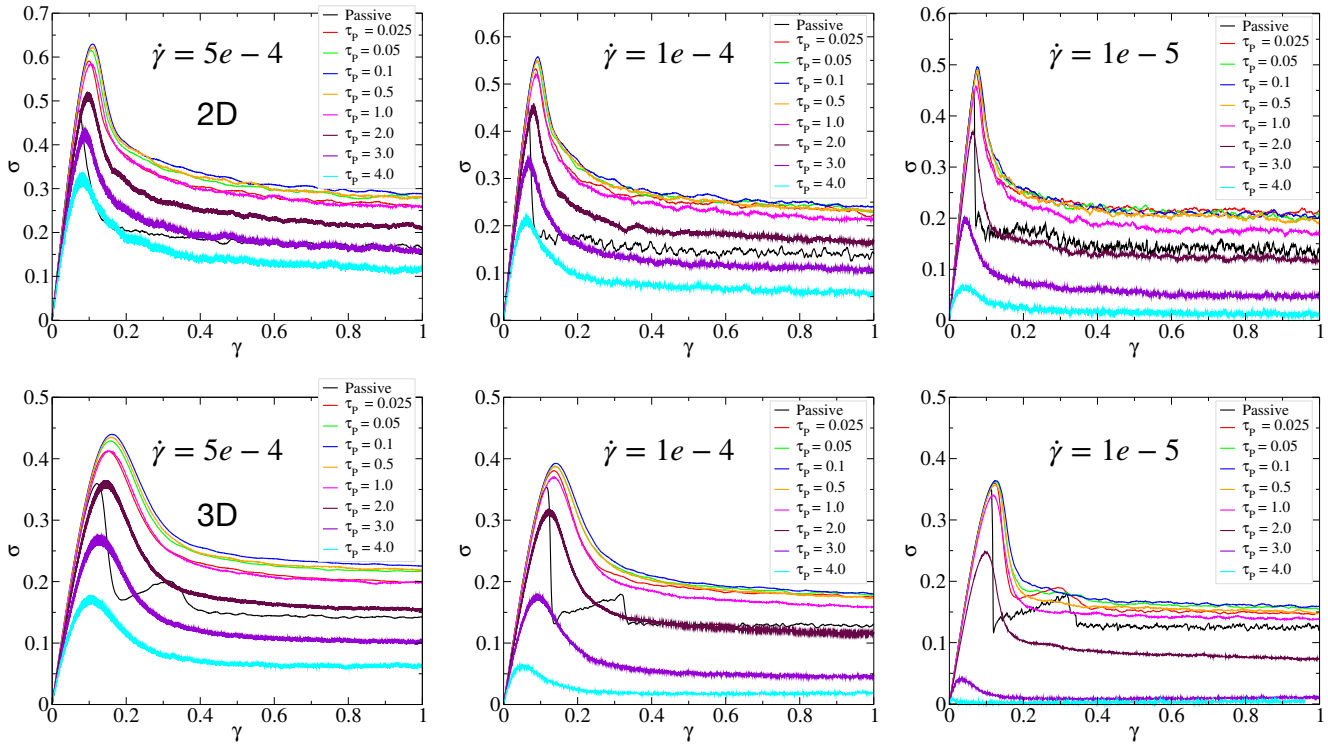

FIG. 11. **Non-Monotonic Yielding with τ_p at Different Strain Rates:** The stress-strain curve for $f_0 = 2.0$ is shown at a strain rates: $\dot{\gamma} = 5 \times 10^{-4}, 1 \times 10^{-4}, 1 \times 10^{-5}$. The top panel displays the results for 2D, while the bottom panel shows the results for 3D. This figure confirms that the non-monotonicity behavior is independent of the strain rate and is consistently present in the system. However, the value of τ_p at which the stress overshoot transitions to an undershoot varies; a larger strain rate corresponds to a larger τ_p value up to which the stress overshoot is observed.

the first data point, which corresponds to the passive system for a given strain rate. $\tau_p = 0$, refers to the passive system, while the middle point corresponds to the maximum observed increase in yield stress and the last point marks the first instance where it decreases relative to the passive system. The data shows that curves at faster strain rates (black) correspond to larger τ_p values, while curves at slower strain rates (blue) correspond to lower τ_p values. The heatmap reveals a decrease in yield stress as the color transitions from red, emphasizing that the correct combination of strain rates, τ_p and f_0 is crucial for enhancing the mechanical response of the system.

The mean square displacement (MSD) of the system, when plotted for different f_0 values at two distinct τ_p values $0.1, 2.0$, shows differences only in the diffusive regime as seen in Fig. 13. However, at a larger persistence time ($\tau_p = 2.0$), the system transitions from ballistic to diffusive smoothly, indicating that the particles, due to increased mobility, can escape cages.

VII. EVOLUTION OF SPACING BETWEEN SHEAR BANDS

We show the evolution of separation between shear band networks with increasing strain at different τ_p values:

- (a) and (c) for $\tau_p = 0.1$ in 2D and 3D, respectively
- (b) and (d) for $\tau_p = 2.0$ in 2D and 3D, respectively

To find the separation between two shear bands we replicate the binary image of the system in 2D as shown in Fig. 4. Many lines are drawn in the horizontal and vertical directions. Along each line, the separation length between shear bands is measured by first identifying shear band regions where D^2_{min} exceeds the cutoff. Whenever D^2_{min} falls below the cutoff, we mark that as the end of a shear band region and continue to measure the separation length from this point until D^2_{min} exceeds the cutoff again, indicating entry into the next shear band. Referring to Fig. 4, the length of the blue regions along the line is measured. The first moment of this length ξ, is then averaged over all ensembles.

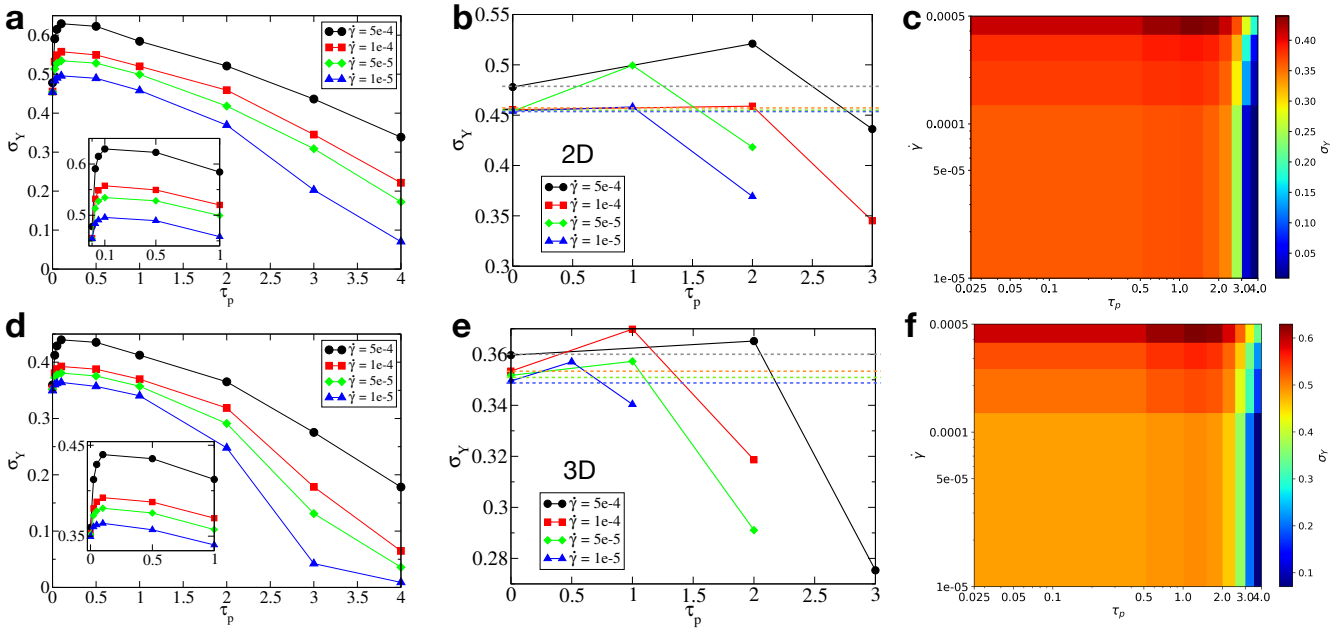

FIG. 12. **Yield Stress for Different τ_p:** The panels (a) and (d) present the yield stress (σ_Y) as a function of the persistence time τ_p for different strain rates ($\dot{\gamma} = 5 \times 10^{-4}, 1 \times 10^{-4}, 5 \times 10^{-5}, 1 \times 10^{-5}$) in 2D and 3D systems respectively. Panels (b) and (e) present zoomed-in views of (a) and (d), focusing specifically on the data points where the yield stress is slightly above and slightly below the reference passive yield stress value. The reference passive yield stress is indicated by the dotted line at various strain rates. These panels highlight that the τ_p value, up to which an increase in yield stress is observed, increases with higher strain rates. Panels (c) and (f) present heatmaps of the yield stress as a function of τ_p for increasing $\dot{\gamma}$, and we see the decrease in yield stress as τ_p approaches > 2.0 in 2D and 3D, respectively. These plots illustrate how the relationship between τ_p, strain rate, and yield stress transitions between 2D and 3D systems.

In Fig. 14, we show the ξ/L with increasing strain, where $L = 100$. Initially, the separation starts at 1.0, as no shear bands are present. It then drops instantly in the passive case as shear bands form, while in active cases, the decrease is more gradual. In the passive system, the separation continues to decrease as the shear bands grow. In active cases, it also decreases initially but eventually saturates due to system size constraints, when the shear band network spans most of the simulation box.

Additionally, we observe that with increasing f_0, the separation between shear bands near yielding and in the transient steady-state decreases. As the shear band network becomes denser, the separation between shear bands $\xi/L \to 0$. However, at $\tau_p = 2.0$ and larger f_0, the system does not form shear bands but rather shows mobile regions homogeneously distributed throughout the system. Consequently, $\xi/L \to 0$ at smaller deformation, which is clearly visible in 3D.

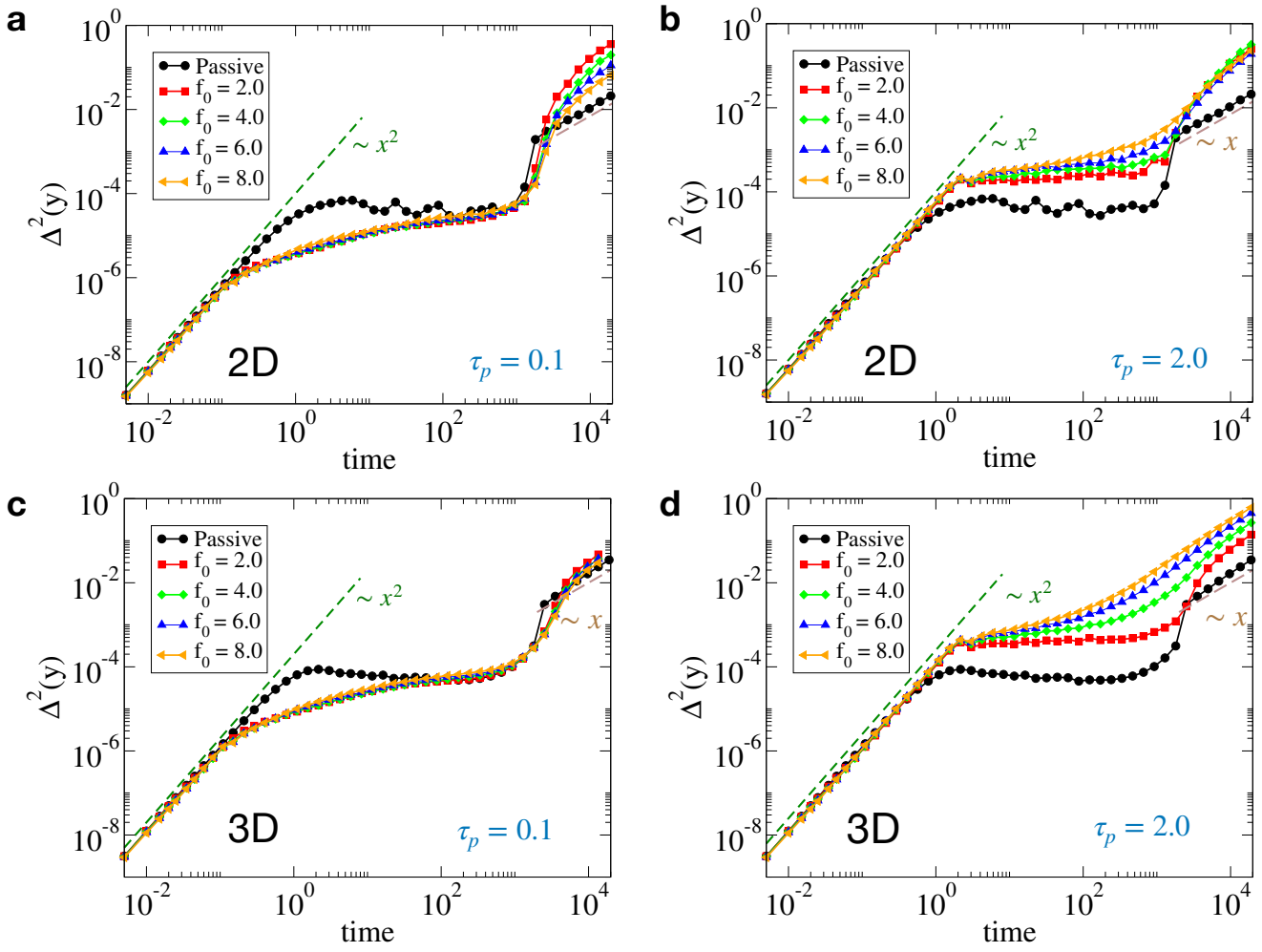

FIG. 13. **Mean Square Displacement (MSD):** This figure shows the mean square displacement (MSD) of particles in the shear perpendicular direction for 2D (top panel) and 3D (bottom panel) systems at a strain rate of $\dot{\gamma} = 5 \times 10^{-5}$, f_0 at different τ_p values $(0.1, 2.0)$. For $\tau_p = 0.1$, the effect of increasing f_0 is noticeable only in the diffusive regime, as there is no prior cage-breaking event. However, for $\tau_p = 2.0$, cage-breaking occurs earlier, and the impact of increasing f_0 is evident sooner. Particles transition directly from the ballistic to the diffusive regime, bypassing the cage with increasing f_0.

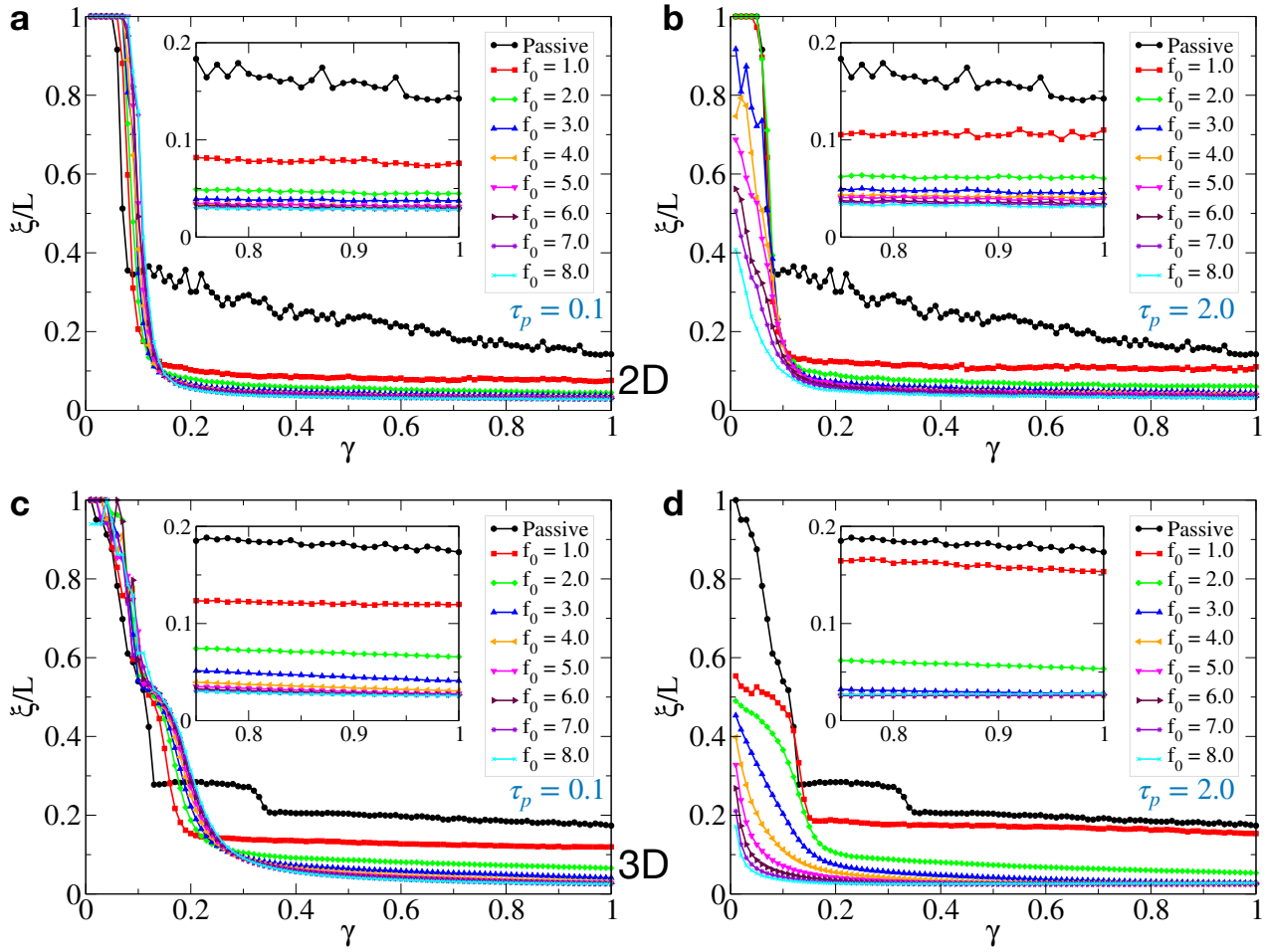

FIG. 14. **Evolution of Distance Between Shear Bands:** This figure illustrates the evolution of the separation between shear bands for different τ_p values $0.1, 2.0$ in 2D (top) and 3D (bottom) systems. The results show that the distance decreases over time, indicating that the shear bands grow and expand as time progresses.